Diffusion Path of Oxide Ions in an Oxide Ion Conductor $La_{0.64}(Ti_{0.92}Nb_{0.08})O_{2.99}$ with a Double Perovskite-Type Structure

Roushown Ali,[†,‡,§] Masatomo Yashima,*[,‡] and Fujio Izumi[†]

Quantum Beam Center, National Institute for Materials Science, 1-1 Namiki, Tsukuba, Ibaraki 305-0044, Japan, and Department of Materials Science and Engineering, Interdisciplinary Graduate School of Science and Engineering, Tokyo Institute of Technology, 4259 Nagatsuta-cho, Midori-ku, Yokohama 226-8502, Japan

Received February 2, 2007. Revised Manuscript Received April 7, 2007

Densities of coherent-scattering lengths in an oxide ion conductor $La_{0.64}(Ti_{0.92}Nb_{0.08})O_{2.99}$ with a double perovskite-type structure (space group *P*4/*mmm*) are determined using neutron powder diffraction data by a whole-pattern fitting approach based on the maximum-entropy method. At temperatures of 496 °C, 1008 °C, and 1358 °C, oxide ions at the 4i site (1/2, 0, *z*) are largely distributed along the ⟨101⟩ directions near the stable positions. The spatial distribution of these oxide ions becomes larger with an increase of temperature. These oxide ions migrate to nearest-neighbor 4i sites along the [100] and [010] directions near the (004) planes at 1008 °C and 1358 °C, corresponding to the spatial dispersion of oxide ions from close to the 4i site onto a wide area of the (004) plane with increasing temperature. The two dimensionality of diffusion paths is attributable to the layered structure of the double perovskite-type $La_{0.64}(Ti_{0.92}Nb_{0.08})O_{2.99}$ compound.

Introduction

Materials with high oxide ion conductivities have received special attention in recent years owing to the potential applications of such materials in batteries and solid-oxide fuel cells and interest in ion-conduction phenomena in crystalline solids.[1−8] Information on the diffusion path and positional disorder of mobile oxide ions at high temperatures, where the materials work most efficiently, is indispensable for developing better oxide ion conductors.[1,7,8] Some perovskite-related ABO_3 phases have high oxide ion conductivity, where A and B denote large and small cations. The present authors have reported the diffusion path of mobile oxide ions in the solid solution of cubic perovskite-type lanthanum gallate $(La_{0.8}Sr_{0.2})(Ga_{0.8}Mg_{0.15}Co_{0.05})O_{2.8}$.[1] However, although there is a wide variety of perovskite-related structures (e.g., A-site deficient double perovskite-type structure), there have been no reports on diffusion paths in such materials.

The lanthanum titanate solid solution $La_{(2\pm x)/3}(Ti_{1-x}M_x)O_{3-\delta}$ (M = Al or Nb, $0.05 \le x \le 0.20$) has an A-site deficient

Table 1. Refined Crystal Parameters and Reliability Factors in Rietveld and MPF Analyses for $La_{0.64}(Ti_{0.92}Nb_{0.08})O_{2.99}$

		temperature		
atom	parameter	496 °C	1008 °C	1358 °C
	a (Å)	3.8827(2)	3.9019(2)	3.9172(2)
	c (Å)	7.8684(4)	7.9118(4)	7.9249(5)
La1	U ($\times 10^{-2}$ Å^2)	1.33(7)	2.83(9)	3.99(12)
La2	U ($\times 10^{-2}$ Å^2)	0.8(2)	1.9(3)	1.3(3)
Ti, Nb	***z***	0.2625(6)	0.2640(7)	0.2621(9)
	U ($\times 10^{-2}$ Å^2)	0.54(10)	1.95(12)	2.51(14)
O1	U_{11} ($\times 10^{-2}$ Å^2)	2.5(2)	4.5(2)	5.1(3)
	U_{33} ($\times 10^{-2}$ Å^2)	1.3(3)	2.3(3)	2.8(4)
	U_{eq} ($\times 10^{-2}$ Å^2)	2.12	3.76	4.32
O2	U_{11} ($\times 10^{-2}$ Å^2)	3.7(2)	5.5(2)	6.4(3)
	U_{33} ($\times 10^{-2}$ Å^2)	0.2(2)	1.1(3)	1.9(4)
	U_{eq} ($\times 10^{-2}$ Å^2)	2.58	4.05	4.91
O3	*z*(O3)	0.2340(3)	0.2344(4)	0.2373(5)
	U_{11} ($\times 10^{-2}$ Å^2)	2.6(2)	4.4(2)	5.6(3)
	U_{22} ($\times 10^{-2}$ Å^2)	0.11(10)	1.04(11)	1.53(14)
	U_{33} ($\times 10^{-2}$ Å^2)	3.16(12)	4.81(14)	5.9(2)
	U_{eq} ($\times 10^{-2}$ Å^2)	1.97	3.41	4.36
reliability factors[a]		$R_{wp} = 5.76\%$, $R_p = 4.28\%$ goodness of fit: 3.16	$R_{wp} = 5.21\%$, $R_p = 3.83\%$ goodness of fit: 2.87	$R_{wp} = 5.00\%$, $R_p = 3.73\%$ goodness of fit: 2.82
		$R_I = 5.38\%$, $R_F = 3.59\%$	$R_I = 4.19\%$, $R_F = 4.36\%$	$R_I = 4.33\%$, $R_F = 5.06\%$
reliability factors[b]		$R_I = 6.03\%$, $R_F = 3.27\%$	$R_I = 4.17\%$, $R_F = 3.13\%$	$R_I = 4.05\%$, $R_F = 3.33\%$

[a] Reliability factors in Rietveld analysis. [b] Reliability factors in MPF. Tetragonal space group *P*4/*mmm* (No. 123), $Z = 2$. *U*, atomic displacement parameter; *z*, fractional coordinate. Occupancies for La1, La2, O1, O2, and O3 sites are assumed to be 1.0, 0.271, 1.0, 0.9972, and 0.9972, respectively. Occupancies of Ti and Nb atoms at the Ti, Nb site are assumed to be 0.9209 and 0.0791, respectively. In analyses, the atom positions were La1 1a (0, 0, 0); La2 1b (0, 0, 1/2); Ti,Nb 2h (1/2, 1/2, *z*); O1 1c (1/2, 1/2, 0); O2 1d (1/2, 1/2, 1/2); and O3 4i (1/2, 0, *z*). Site symmetries give constraints $U_{12} = U_{13} = U_{23} = 0$ at the O1, O2, and O3 sites and $U_{11} = U_{22}$ at the O1 and O2 sites. Only independent atomic displacement parameters are given.

* To whom all correspondence should be addressed. E-mail: yashima@materia.titech.ac.jp.
† National Institute for Materials Science.
‡ Tokyo Institute of Technology.
§ Permanent address: Department of Chemistry, University of Rajshahi, Rajshahi-6205, Bangladesh.

(1) Yashima, M.; Nomura, K.; Kageyama, H.; Miyazaki, Y.; Chitose, N.; Adachi, K. *Chem. Phys. Lett.* **2003**, *380*, 391.
(2) Boivin, J. C.; Mairesse, G. *Chem. Mater.* **1998**, *10*, 2870.
(3) Islam, M. S. *J. Mater. Chem.* **2000**, *10*, 1027.
(4) Lacorre, P.; Goutenoire, F.; Bohnke, O.; Retoux, R.; Laligant, Y. *Nature* **2000**, *404*, 856.
(5) Hayashi, H.; Inaba, H.; Matsuyama, M.; Lan, N. G.; Dokiya, M.; Tagawa, H. *Solid State Ionics* **1999**, *122*, 1.
(6) Inaba, H.; Tagawa, H. *Solid State Ionics* **1996**, *83*, 1.
(7) Yashima, M.; Ishimura, D. *Chem. Phys. Lett.* **2003**, *378*, 395.
(8) Yashima, M.; Ishimura, D. *Appl. Phys. Lett.* **2005**, *87*, 221909.

10.1021/cm070321a CCC: $37.00
Published on Web 06/05/2007

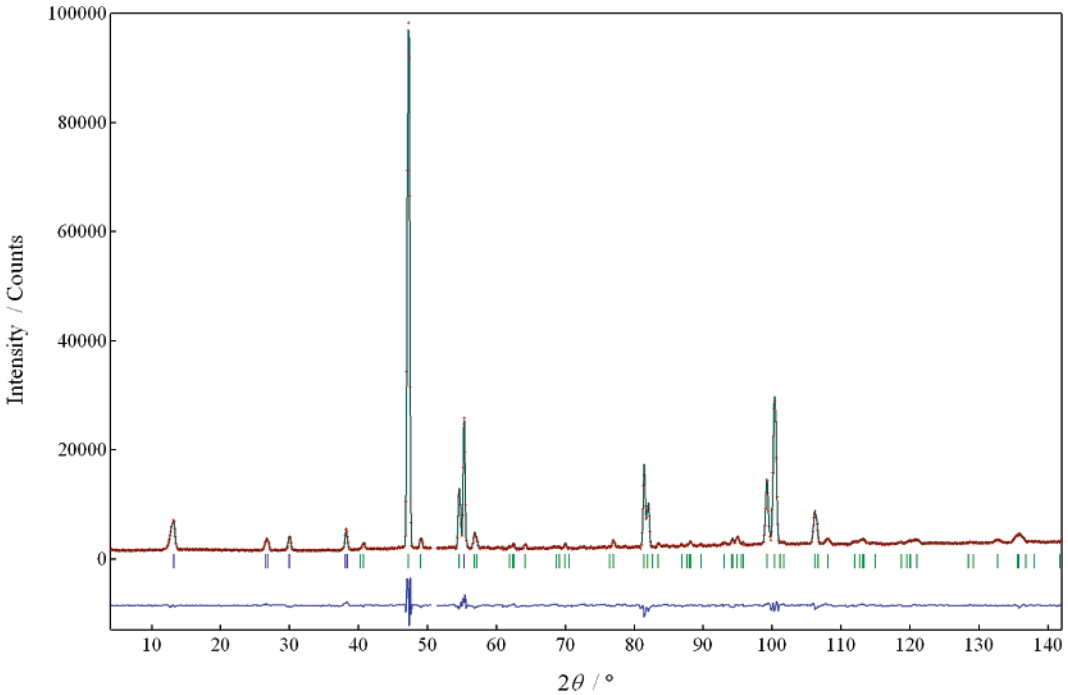

Figure 1. Rietveld fitted pattern of neutron powder diffraction data for $La_{0.64}(Ti_{0.92}Nb_{0.08})O_{2.99}$ at 1358 °C (wavelength of neutron = 1.8143 Å). Crosses and lines denote observed and calculated profile intensities, respectively. Short vertical bars represent Bragg reflection positions. The difference (observed − calculated) is plotted below the profile.

perovskite-type structure[9−18] and exhibits high oxide ion conductivity at high temperature.[9−12] Here the δ is the concentration of oxygen defects. These compounds have a perovskite-type structure with double unit cell along the *c*-axis at high temperatures above the orthorhombic−tetragonal transition point, and the crystal structure and structural phase transitions of $La_{(2-x)/3}(Ti_{1-x}M_x)O_{3-\delta}$ have been studied extensively.[11,13−22] It is therefore of interest to compare the diffusion path in such an A-site deficient layered perovskite-type compound having a double unit cell along the *c*-axis with that in the ideal cubic perovskite-type material.

Yoshioka[10] studied the electrical properties of $La_{(2\pm x)/3}(Ti_{1-x}Nb_x)O_{3-\delta}$ ($x = 0.05-0.15$) and reported that a sample with $x = 0.10$ displayed the highest ionic conductivity (10^{-2} S cm^{-1} at ca. 700 °C) of the samples examined. In the present study, the crystal structure and pathway of oxide ion diffusion in $La_{0.64}(Ti_{0.92}Nb_{0.08})O_{3-\delta}$ ($x = 0.08$) are examined at high temperature. The pathway of oxide ion diffusion is visualized using neutron powder diffraction data and a whole-pattern fitting (wpf) approach based on the maximum-entropy method (MEM).[1,7,8,23−26] Neutron diffraction data are utilized because of the relatively high contributions of oxygen atoms to diffraction intensities in $La_{0.64}(Ti_{0.92}Nb_{0.08})O_{3-\delta}$ containing heavy-metal atoms. MEM-based pattern fitting (MPF)[1,7,8,25,26] is also effective for determination of the spatial distribution of mobile oxide ions in highly disordered structures.

Experimental Procedures

The $La_{0.64}(Ti_{0.92}Nb_{0.08})O_{2.99}$ specimen was prepared by solid-state reactions from high-purity powders of La_2O_3, TiO_2, and Nb_2O_5 (>99.9%).[15] The powders were well mixed and ground in an agate mortar for 90 min as both dry powders and ethanol slurries. The mixture was pressed into pellets under pressure of 100 MPa and sintered at 1350 °C for 19 h in air. A part of each sintered pellet was crushed and ground into powder for characterization by X-ray powder diffraction using a RINT 2550V/PC diffractometer. The resulting X-ray powder diffraction patterns revealed the sample to consist of a single orthorhombic *Cmmm* phase without impurities such as $LaTiNbO_6$ or $La_2Ti_2O_7$.[15] Inductively coupled plasma optical emission spectroscopy chemical analyses indicated that the chemical formula of the final product was $La_{0.636(1)}(Ti_{0.921}Nb_{0.079(1)})O_{2.993(1)}$ where the number in parenthesis is the error in the last digit. The value for oxygen 2.993 was calculated by the electrical neutrality and suggests a small amount of oxygen defects.

Neutron powder diffraction data for $La_{0.64}(Ti_{0.92}Nb_{0.08})O_{2.99}$ were collected at 496 °C, 1008 °C, and 1358 °C using the HERMES

(9) Suvorov, D.; Valant, M.; Skapin, S.; Dolar, D. *J. Mater. Sci*. **1998**, *33*, 85.
(10) Yoshioka, H. *J. Am. Ceram. Soc*. **2002**, *85*, 1339.
(11) Yoshioka, H.; Kikkawa, S. *J. Mater. Chem*. **1998**, *8*, 1821.
(12) Yoshioka, H. *Jpn. J. Appl. Phys*. **1994**, *33* (Part 2), L945.
(13) Yashima, M.; Ali, R.; Yoshioka, H. *Solid State Ionics* **2000**, *128*, 105.
(14) Ali, R.; Yashima, M.; Yoshimura, M.; Yoshioka, H. *J. Am. Ceram. Soc*. **2001**, *84*, 468.
(15) Yashima, M.; Mori, M.; Kamiyama, T.; Oikawa, K. I.; Hoshikawa, A.; Torii, S.; Saitoh, K.; Tsuda, K. *Chem. Phys. Lett*. **2003**, *375*, 240.
(16) Ali, R.; Yashima, M.; Tanaka, M.; Yoshioka, H.; Mori, Y.; Sasaki, S. *J. Solid State Chem*. **2002**, *164*, 51.
(17) Skapin, S.; Kolar, D.; Suvorov, D. *J. Am. Ceram. Soc*. **1993**, *76*, 2359.
(18) Petzelt, J.; Buixaderas, E.; Komandin, G.; Pronin, A. V.; Valant, M.; Suvorov, D. *Mater. Sci. Eng*. **1998**, *B57*, 40.
(19) Slater, P. R.; Irvine, J. T. S. *J. Solid State Chem*. **1999**, *146*, 437.
(20) Yashima, M.; Mori, M.; Ali, R.; Tanaka, M.; Mori, T. *Chem. Phys. Lett*. **2003**, *371* 582.
(21) Yashima, M.; Ali, R.; Tanaka, M.; Mori, T. *Chem. Phys. Lett*. **2002**, *363*, 129.
(22) Ali, R.; Yashima, M. *J. Synchrotron Rad*. **2003**, *10*, 228.
(23) Collins, D. M. *Nature* **1982**, *298*, 49.
(24) Takata, M.; Umeda, B.; Nishiborai, E.; Sakata, M.; Saito, Y.; Ohno, M.; Shinohara, H. *Nature* **1995**, *377*, 46.
(25) Izumi, F.; Kumazawa, S.; Ikeda, T.; Hu, W.-Z.; Yamamoto, A.; Oikawa, K. *Mater. Sci. Forum* **2001**, *378−381*, 59.
(26) Izumi, F.; Dilanian, R. A. *Recent Res. Dev. Phys*. **2002**, *3*, 699.

powder diffractometer[27] installed at the JRR-3M research reactor of the Japan Atomic Energy Agency, Tokai, Japan. Incident neutrons with a fixed wavelength of 1.8143 Å were obtained using a vertically focusing (331) Ge monochromator. The powder diffraction data were measured over a 2θ range of 3−152.62° using 150 ^{3}He counters. The sample was heated at a rate of 10 °C/min using a furnace with $MoSi_2$ heaters.[28] The temperature of the sample was maintained within ±1.5 °C during each measurement.

The diffraction data were analyzed by the Rietveld method followed by application of MPF using the computer programs RIETAN-2000[29] and PRIMA.[26] A split-type pseudo-Voigt profile function formulated by Toraya[30] was used in the Rietveld refinements. The cutoff value was 7.00 × (full-width at half-maximum). A Legendre polynomial function with 12 parameters was fitted to background intensities. The coherent scattering lengths (b_c) adopted for Rietveld refinement were 8.24 fm for La, −3.37 fm for Ti, 7.054 fm for Nb, and 5.805 fm for O.

Results and Discussion

All reflections in the neutron powder diffraction patterns for $La_{0.64}(Ti_{0.92}Nb_{0.08})O_{2.99}$ at 496 °C, 1008 °C, and 1358 °C were indexed on the basis of a tetragonal *P*4/*mmm* cell ($a = b \approx a_p$, $c \approx 2a_p$; subscript p denotes the pseudo-cubic perovskite-type structure), consistent with previous work.[15] The X-ray diffraction profile at room temperature indicates a single orthorhombic phase. The orthorhombic *Cmmm* phase transformed into the tetragonal symmetry at 350 °C during heating.[15,16] In a preliminary analysis, the site occupancies at the La1 1a (0, 0, 0) site *g*(La1) and at the La2 1b (0, 0, 1/2) site *g*(La2) were refined under the constraint of the chemical composition ($g(La2) = 1.271 - g(La1)$), which suggested that the *g*(La1) site is fully occupied. Therefore, the occupancies of La1 and La2 were fixed at 1.0 and 0.271, respectively, in the subsequent refinements at 496 °C, 1008 °C, and 1358 °C (Table 1). Rietveld analysis with the fixed occupancy factors gave no significant variations of the refined parameters. The occupancy factors $g(La1) = 1.0$ and $g(La2) = 0.271$ are consistent with those ($g(La1) = 0.996(4)$, $g(La2) = 0.284(4)$) reported by Yashima et al.[15] within the estimated standard deviation. Yashima et al.[15] also concluded that the occupancies at the La1 and La2 sites were independent of temperature in the range 25−467 °C. In other preliminary analyses, the occupancies of oxygen atoms at the O1, O2, and O3 sites were refined, which suggested that the O1 site is fully occupied and that the O2 and O3 sites have small amounts of deficiency. Therefore, the occupancies at the O1, O2, and O3 sites are assumed to be 1.00, 0.9972, and 0.9972, respectively. The value 0.9972 was estimated with the chemical analysis results and electrical neutrality. Refinements of anisotropic atomic displacement parameters (U_{ij}) for cations resulted in no significant improvement in the reliability (*R*) factors. Therefore, U_{ij} were refined only for oxygen sites in subsequent Rietveld refinements. The technique of partial profile relaxation[29,31] was applied to seven reflections, which significantly improved fits between observed and calculated profiles for these reflections (Figure 1). The refined unit-cell and structural parameters and *R* factors are summarized in Table 1. The unit-cell parameters increased with temperature. The unit-cell volume also increased with temperature as a result of thermal expansion.

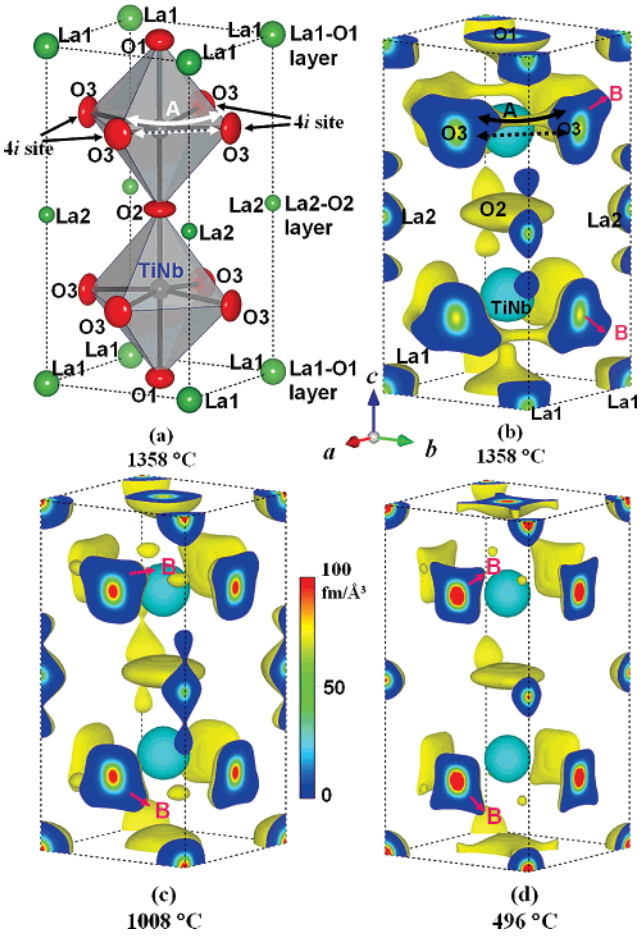

Figure 2. (a) Refined crystal structure of double perovskite-type $La_{0.64}(Ti_{0.92}Nb_{0.08})O_{2.99}$, and (b−d) equi-density surface of scattering-length density distribution at 0.1 fm Å^{-3} and scattering-length density on the (100), (010) and (001) planes in $La_{0.64}(Ti_{0.92}Nb_{0.08})O_{2.99}$ at 1358 °C (b), 1008 °C (c), and 496 °C (d). Oxygen atoms at the O3 site have a large spatial distribution to the ⟨101⟩ directions shown by the line with an arrow (B). The O3 atoms do not move along the straight line shown by the dotted line with arrows but along the curved solid line with arrows (A).

Figure 2a shows the crystal structure of the $La_{0.64}(Ti_{0.92}Nb_{0.08})O_{2.99}$ compound with the refined crystallographic parameters. This is the high-temperature form of $La_{0.64}(Ti_{0.92}Nb_{0.08})O_{2.99}$, which has an A-site deficient perovskite-type structure with double perovskite ABO_3 units along the *c*-axis ($Z = 2$), where A = $La_{0.64}$ and B = $(Ti_{0.92}Nb_{0.08})$. The occupancy factors of La at the La1 and La2 sites are $g(La1) = 1.00$ and $g(La2) = 0.271$. The dissimilarity of these values reflects the chemical ordering of occupied La1 and defective La2 sites (Figure 2a). The Ti and Nb atoms exhibited a shift from the regular position ($z = 1/4$ and 3/4) toward the La-deficient La2−O2 layer along the *c*-axis (Table 1). The magnitude of the shift did not change with increasing temperature. The *z* coordinate of the O3 atom was smaller than 1/4 and remained largely unchanged with varying temperature (Table 1). All the refined atomic displacement parameters increased with temperature (Table 1). The atomic

(27) Ohoyama, K.; Kanouchi, T.; Nemoto, K.; Ohashi, M.; Kajitani, T.; Yamaguchi, Y. *Jpn. J. Appl. Phys.* **1998**, *37* (Part 1), 3319.
(28) Yashima, M. *J. Am. Ceram. Soc.* **2002**, *85*, 2925.
(29) Izumi F.; Ikeda, T. *Mater. Sci. Forum* **2000**, *321*−*324*, 198.
(30) Toraya, H. *J. Appl. Crystallogr.* **1990**, *23*, 485.
(31) Izumi, F. *Rigaku J.* **2000**, *17*, 34.

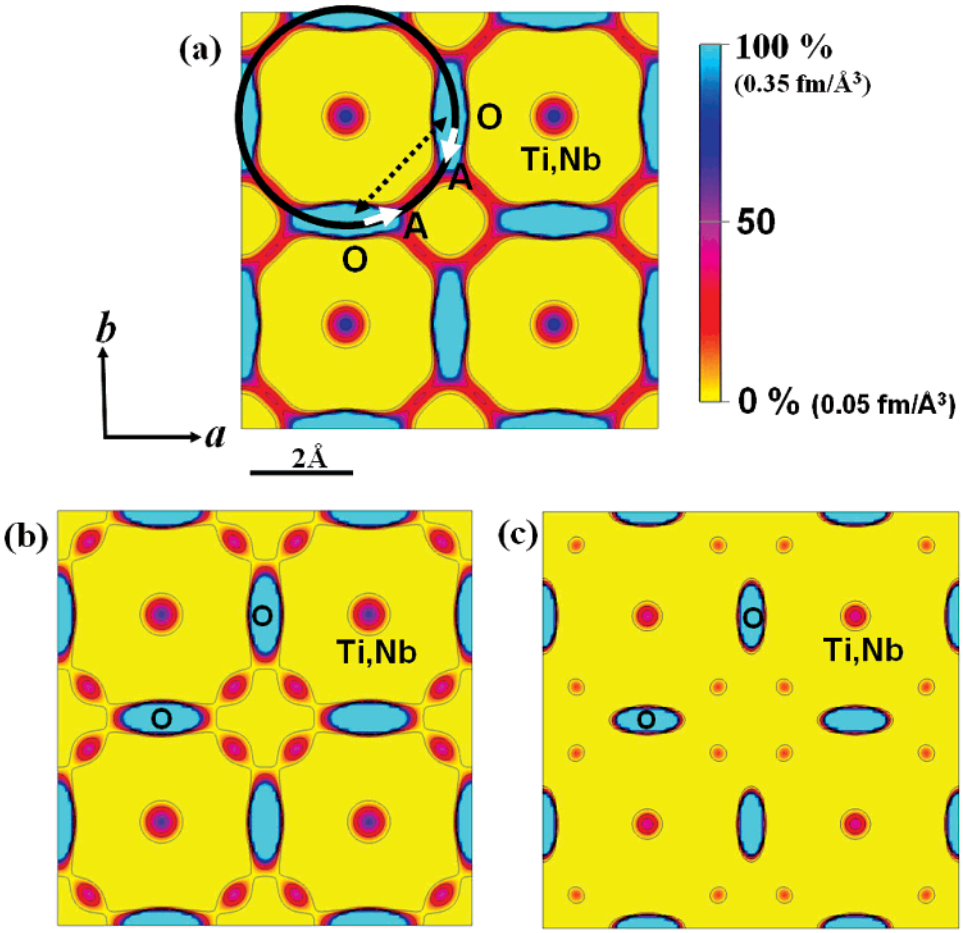

Figure 3. Distribution of absolute scattering-length densities on the *ab* plane at $z = 0.2$ ($0 < x, y < 2$) of double perovskite-type *P4/mmm* $La_{0.64}(Ti_{0.92}Nb_{0.08})O_{2.99}$ at (a) 1358 °C, (b) 1008 °C, and (c) 496 °C in the range of 0.05−0.35 fm Å^{-3}. Contours in the range of 0.05−0.35 fm Å^{-3} are increased by the step of 0.05 fm Å^{-3} contours. The solid line in part (a) denotes a curved diffusion path of oxide ions, and the dotted line denotes a direct path between ideal positions. At low temperature (496 °C), oxide ions are localized near the equilibrium position (see part c); at high temperature (1358 °C), the oxide ions are dispersed over a wide area between the regular positions (see part a).

displacement parameters for oxygen atoms were larger than for the cations, suggesting a larger diffusion coefficient for oxide ions. The oxygen atoms also displayed large anisotropy in the atomic displacement parameters, suggesting a directionality in the movements of oxide ions around the stable positions. Similar large and anisotropic thermal motions of oxide ions have been observed for the cubic perovskite-type oxide ion conductor $(La_{0.8}Sr_{0.2})(Ga_{0.8}Mg_{0.15}Co_{0.05})O_{2.8}$.[1]

MEM analysis was conducted using diffraction data in the 2θ range of 4.0−140°, corresponding to $d > 1.0$ Å (d: spacing of lattice planes), with the structure factors obtained from Rietveld analysis. A total of 59 structure factors were obtained for all data measured at the three different temperatures. The 001 reflection appearing at the lowest 2θ position (ca. 13°) was included, as that peak provides information on the disordered arrangements of oxide ions. The MEM calculations were performed using PRIMA with the unit cell divided into 64 × 64 × 128 pixels, coupled with wpf by RIETAN-2000.[29] To reduce the bias imposed on the nuclear density by the simple structural model adopted in the Rietveld analyses, an iterative procedure called the REMEDY cycle[25,26] was employed following MEM analyses. In REMEDY cycles, structure factors, F_c(MEM), were calculated by the Fourier transform of nuclear densities resulting from MEM analysis. In the subsequent wpf, structure factors F_c(MEM) obtained in the previous MEM analysis were fixed, and parameters irrelevant to the structure, for example, scale factor, profile, lattice, and background parameters, were refined by RIETAN-2000.[29] Observed structure factors F_o-(wpf) evaluated after wpf were analyzed again by the MEM. In this way, wpf and MEM analyses were alternately repeated (REMEDY cycles) until the reliability indices no longer decreased. Use of the REMEDY cycle resulted in significant improvement in the R factors based on the Bragg intensities (R_I) and structure factors (R_F; Table 1). Figure 2b,c,d shows the equi-density surface and nuclear-density distributions on the (100), (010) and (001) planes of the $La_{0.64}(Ti_{0.92}Nb_{0.08})$-$O_{2.99}$ obtained after the REMEDY cycle. Figure 3 shows the temperature dependence of the nuclear density contour map at $z = 0.2$ on the *ab* plane. Figures 2b−d and 3 provide much information on the positional disorder and diffusion path of the mobile oxide ions compared to the simple atomistic model (Figure 2a).

At 496 °C, the O3 atoms are localized near the stable 4i site (1/2, 0, 0.234). The O3 atoms display small bulges in the ⟨101⟩ direction (B in Figure 2d), which become larger at 1008 °C and 1358 °C (Figure 2b,c). The probability density of an O3 atom is connected with that of nearest-neighbor O3 atoms, indicating diffusion along a pathway following the [100] and [010] directions (A in Figure 2b).

The O3 atoms migrate to the nearest-neighbor 4i site through a triangle formed by adjacent La1, La2, and Ti, Nb atoms. The spatial distribution of the O3 atoms becomes larger with an increase of temperature (Figures 2 and 3). Such an increase in the density of oxide ions with increasing temperature is consistent with the higher conductivity at higher temperatures.[10]

The O3 atom migrates following a curved route so as maintain a relatively constant distance from Ti, Nb atoms (solid curve with arrows A in Figures 2a,b and 3), rather than a direct linear path (straight dotted lines with arrows between regular positions in Figures 2a,b and 3a). Yashima et al.[1] in their study of the nuclear density distribution of an ideal cubic perovskite-type compound $(La_{0.8}Sr_{0.2})(Ga_{0.8}Mg_{0.15}Co_{0.05})O_{2.8}$ found similar curved migration pathways. Computer simulations[3,32] for the perovskite-structured $LaBO_3$ (B = Co, Mn, Ga, Cr, and Fe) compounds have also revealed deviation of the migration pathway from the direct path. The curved feature in the migration paths was also found in the nuclear and electron density distribution maps of the lithium cation conductor $La_{0.62}Li_{0.16}TiO_3$,[33] the fluorite-type structured anion conductors $Bi_{1.4}Yb_{0.6}O_3$[8] and $Ce_{0.93}Y_{0.07}O_{1.96}$,[34] and the fluorite-type structured Cu cation conductor CuI.[35] The present work has demonstrated the presence of a curved diffusion pathway in double perovskite-type structured oxide ion conductors for the first time.

The oxide ion conductor with an ideal perovskite-type structure exhibits diffusion paths along the [100], [010], and [001] directions to form a three-dimensional network of equivalent diffusion pathways, as shown by Yashima et al.[1] On the contrary, in the present double perovskite-type $La_{0.64}(Ti_{0.92}Nb_{0.08})O_{2.99}$, a two-dimensional diffusion pathway is present, by which O3 atoms migrate along the [100] and [010] directions (Figure 2b,c). This two-dimensional feature is attributable to the layered structure of the $La_{0.64}(Ti_{0.92}Nb_{0.08})O_{2.99}$, which consists of La-occupied La1−O1, (Ti,Nb)−O, and La-deficient La2−O2 layers. Two-dimensional lithium cation conduction has also been reported in the orthorhombic layered perovskite-type compound $La_{0.62}Li_{0.16}TiO_3$,[33,36−38] where the Li cation is able to exist and migrate only on the La deficient La2−O2 layer. The present work has thus revealed the two-dimensional feature of oxide ion diffusion.

Acknowledgment. We thank Mr. S. Takenouchi and Dr. Y. Matsushita (NIMS) for their help with ICP analyses. The authors would like to thank Dr. K. Ohoyama and Mr. K. Nemoto for use of the HERMES diffractometer. Special thanks are extended to Mr. M. Mori for sample preparation. Mr. T. Wakita, Mr. Y. Ando, Mr. Q. Xu, Mr. T. Tsuji, Mr. Y. Kawaike, and Mr. T. Ueda are gratefully acknowledged for experimental assistance. This research was supported in part by the Ministry of Education, Culture, Sports, Science and Technology of Japan (Monbu-Kagaku-sho).

CM070321A

(32) Cherry, M.; Islam, M. S.; Catlow, C. R. A. *J. Solid State Chem.* **1995**, *118*, 125.
(33) Yashima, M.; Itoh, M.; Inaguma, Y.; Mori, Y. *J. Am. Chem. Soc.* **2005**, *27*, 3491.
(34) Yashima, M.; Kobayashi, S.; Yasui, T. *Faraday Discuss.* **2007**, *134*, 369.
(35) Yashima, M.; Xu, Q.; Yoshiasa, A.; Wada, S. *J. Mater. Chem.* **2006**, *16*, 4393.
(36) Sanz, J.; Varez, A.; Alonso, J. A.; Fernandez, M. T. *J. Solid State Chem.* **2004**, *177*, 1157.
(37) Inaguma, Y.; Katsumata, T.; Itoh, M.; Morii, Y. *J. Solid State Chem.* **2002**, *166*, 67.
(38) Ibarra, J.; Varez, A.; Leon, C.; Santamaria, J.; Torres-Marinez, L. M.; Sanz, J. *Solid State Ionics* **2000**, *134*, 219.